European Spine Journal (2019) 28:1697–1711
https://doi.org/10.1007/s00586-019-05969-4

ORIGINAL ARTICLE

Implementation of augmented reality support in spine surgery

Barbara Carl[1] · **Miriam Bopp**[1,2] · **Benjamin Saß**[1] · **Benjamin Voellger**[1] · **Christopher Nimsky**[1,2]

Received: 7 September 2018 / Revised: 2 December 2018 / Accepted: 2 April 2019 / Published online: 5 April 2019

Abstract

Purpose To implement a straightforward workflow that allows to establish augmented reality (AR) support in spine surgery.

Methods Intraoperative computed tomography (iCT) applying a 32-slice movable scanner was used for navigation registration in a series of 10 patients who underwent surgery for extra- or intradural spinal lesions. Preoperative multimodal image data were integrated by nonlinear registration with the iCT images. Automatic segmentation was used to delineate the 3-dimensional (3-D) outline of the vertebra, and in addition, the tumor extent, as well as implants, was segmented and visualized.

Results Automatic patient registration without user interaction resulted in high navigation accuracy with a mean registration error of only about 1 mm. Moreover, the workflow for establishing AR was straightforward and could be easily integrated in the normal surgical procedure. Low-dose iCT protocols resulted in a radiation exposure of 0.35–0.98 mSv for cervical, 2.16–6.92 mSv for thoracic, and 3.55–4.20 mSv for lumbar surgeries, which is a reduction in the effective radiation dose by 70%. The segmented structures were intuitively visualized in the surgical field using the heads-up display of the operating microscope. In parallel, the microscope video was superimposed with the segmented 3-D structures, which were visualized in a semitransparent manner along with various display modes of the image data.

Conclusions A microscope-based AR environment was successfully implemented for spinal surgery. The application of iCT for registration imaging ensures high navigational accuracy. AR greatly supports the surgeon in understanding the 3-D anatomy thereby facilitating surgery.

Graphical abstract

These slides can be retrieved under Electronic Supplementary Material.

Keywords Augmented reality · Intraoperative computed tomography · Low-dose computed tomography · Navigation registration · Spine tumor surgery

Introduction

In the 1980s, the first attempts of superimposing information on optical systems which would nowadays be called "augmented reality" (AR) were based on operating microscopes used in cranial neurosurgery. This pioneering work

Electronic supplementary material The online version of this article (https://doi.org/10.1007/s00586-019-05969-4) contains supplementary material, which is available to authorized users.

✉ Barbara Carl
carlb@med.uni-marburg.de

Extended author information available on the last page of the article

enriching the optical information of operating microscopes was undertaken by Kelly [1] and by Roberts [2]. Computed tomography (CT) data were reformatted into a plane and orientation that corresponds to the microscope's focal plane. This information was then projected into the optics of the operating microscope using a miniature cathode ray tube and a beam splitter [2]. In the mid-1990s, these concepts led to the first commercial operating microscopes with heads-up displays integrated in a navigation setup thereby allowing to superimpose outlines of structures in the visual field [3, 4]. In parallel, the use of head-mounted displays was tested [5], as well as the first AR setups for vascular procedures [6]. In recent years, the visualization capabilities integrated in modern operating microscopes improved in conjunction with the software enabling visualization of 3-dimensional (3-D) colored objects [7–9].

However, until now, microscope support was not implemented in the navigation systems for spine surgery. Only recently the first attempts to integrate AR into spine surgery were published. For instance, a 3-D guidance system using AR for percutaneous vertebroplasty was tested [10]. Furthermore, a very recent feasibility study demonstrated the concept of AR to guide lumbar facet joint injections [11]. For pedicle screw placements, AR showed its potential in two cadaver studies [12, 13]. The heads-up display technology of operating microscopes was used to visualize osteotomy planes in a phantom study [14].

The aim of this paper is to demonstrate how we established AR support for spinal surgery and applied this in an initial series of patients with spine lesions.

Materials and methods

Between June and August 2018, 10 patients (5 females, 5 males; age range 31–75 years) underwent surgery for intra- and extradural spinal lesions (Table 1). Informed consent was obtained from all individual participants included in the study. We obtained ethics approval that there is no need for further ethical approval for a retrospective evaluation of prospectively archived routine clinical and technical data.

Operative setting and intraoperative image registration

Standard c-arm X-ray was used prior skin incision for level definition. A movable 32-slice CT scanner (AIRO, Brainlab, Munich, Germany) is used for intraoperative CT (iCT). For iCT, no patient movement is necessary. Details describing the setup are published [9, 15]. The operative setting was identical for all cases, and no modifications to apply the technique for the different parts of the spine were necessary. Scan parameters are summarized in Table 2.

Prior to iCT, the reference array is attached to a spinous process (Fig. 1a). Alternatively, the reference array is taped directly on the skin, when only one or two levels are exposed. In case of lateral positioning, the reference array can be attached to an extra arm or directly to a spinal retractor. ICT is performed after exposing the spine, while the retractors are not removed. To enable automatic registration, scanner and patient are tracked during iCT (Fig. 1a). Registration accuracy is measured by placing the pointer tip on anatomical landmarks like the spinous

Table 1 Patient characteristics

No.	Age (yrs)	Sex	Diagnosis	Procedure	Positioning
1	65	f	Meningioma WHO I intradural C2–C3	Laminectomy C2–C3, complete resection	Prone
2	59	m	Squamous cell lung carcinoma metastasis intra- and extradural C0–C3	Craniotomy posterior fossa, laminectomy C1–C3, resection of intradural tumor	Prone
3	75	f	Breast cancer metastasis vertebral body L2	Posterior fixation L1–L3 and corpectomy L2 and X-core vertebral body replacement L2	Prone and lateral
4	51	m	Lymphoma intradural L1–L3	Laminectomy L1, biopsy	Prone
5	75	m	Small cell lung carcinoma metastasis vertebral bodies T8–T9, partially intraspinal	Posterior fixation T6–T11, hemilaminectomy T8–T9, decompression, biopsy	Prone
6	59	m	Neuroendocrine carcinoma metastasis epidural T6	Laminectomy T6, complete resection	Prone
7	31	f	Benign cystic lesion conus medullaris T11–T12	Partial laminectomy T11, laminectomy T12, cyst drainage	Prone
8	61	f	Adhesive arachnoiditis T3–T4	Laminoplasty T3–T4, intradural decompression	Prone
9	68	f	Mesenchymal chondrosarcoma vertebral body T2 and intraspinal, extradural T6	Posterior fixation T1–T4 and laminectomy T6, decompression, partial resection	Prone
10	64	m	Small cell lung carcinoma metastasis vertebral body T1	Corpectomy T1, X-core mini vertebral body replacement T1 and posterior fixation C7–T2	Supine and prone

f female, *m* male, *WHO* World Health Organization, *yrs* years

Table 2 Scan parameters for iCT

Protocol	Acquisition	Standard mA	kV	Adapted mean mA	Mean CTDIvol (mGy)
Sinus—80%	Axial	7.07	120	7.07	2.70
C-Spine—70%	Helical	28	120	28	5.66
T-Spine—70%*	Helical	33	120	42.82 ± 10.48	8.66 ± 2.12
L-Spine—70%*	Helical	33	120	41.11 ± 5.47	8.32 ± 1.11

CTDIvol computed tomography dose index

*Weight adaption applied (standard weight 70 kg; adapted mA = standard mA * patient weight/standard patient weight)

Fig. 1 Operating room setting: **a** for automatic registration, the navigation camera tracks the scanner (black arrows) and the reference array that is attached to the patient (white arrows); **b** the operating microscope enabling AR is tracked during surgery (black arrows); **c** setting during surgery with the operating microscope where the AR information is superimposed by the integrated heads-up display, additionally the microscope video is shown on screens with an AR overlay, and the autofocus position of the microscope is displayed in co-registered CT and MR images in the spinal navigation application

process, vertebra lamina, or the vertebral body surface, or on artificial landmarks, like attached skin fiducials, retractor arms, reflecting spheres of the registration array, or clips placed in the surgical field.

For calculation of the effective dose (ED), the total dose length product (DLP) was multiplied by ED/DLP conversion factors, which are estimated to be 5.4 µSv/Gy * cm for cervical, 17.8 µSv/Gy * cm for thoracic, and 19.8 µSv/Gy*cm

Table 3 Clinical outcome

No.	Preoperative symptoms	Outcome
1	Ataxia, palsy right hand	Improvement in ataxia and palsy
2	No neurological deficits	No impairment
3	Pain (VAS 7)	Pain relief (VAS 3), no neurological deficits
4	Ataxia, incomplete paraplegia	Incomplete improvement in paraplegia
5	Pain (VAS 9)	Pain relief (VAS 4), no neurological deficits
6	Ataxia	Improvement in ataxia
7	Spastic muscle cramps	Reduction in muscle cramps, no neurological deficits
8	Pain (VAS 6)	Pain relief (VAS 2), no neurological deficits
9	Radiculopathy T1 and T2, ataxia	Improvement in ataxia and pain relief
10	C8 palsy, radiculopathy C8	Improvement in palsy and pain relief

VAS visual analog scale

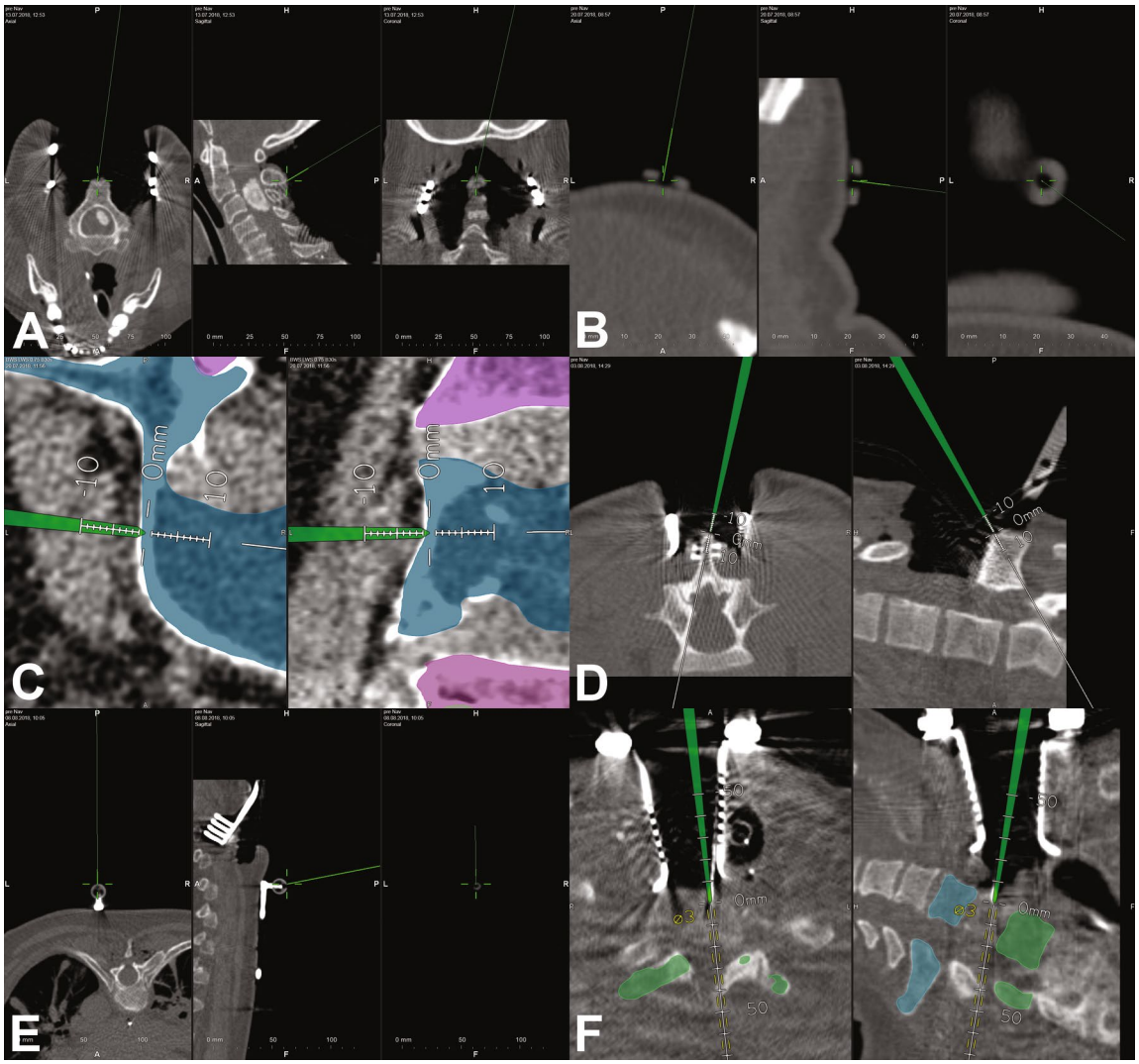

Fig. 2 Examples of how registration accuracy can be checked with the tip of the navigation pointer: **a** on the spinous process; **b** in the divot of skin fiducials; **c** at the bone surface in a lateral approach; **d** on the spinous process close to the reference clamp; **e** on the reflective sphere of the reference array; **f** on a metallic clip placed prior to iCT to check accuracy

Table 4 Image datasets fused with iCT registration scan for integration in navigation and visualized objects in augmented reality

No.	With iCT registration scan fused image sets	Visualized objects in augmented reality
1	CT, MRI (3D-T1, 3D-T2, DWI), iCT2	Tumor, C2, C3, C4, tractography
2	CT, MRI (3D-T1), iUS, iCT2	Tumor, C1, C2, C2, C3, C4, C5, C6
3	CT, MRI (sagittal T1), iCT2	T12, L1, L2, L3, L4, posterior fixation (screws and rods), vertebral body replacement
4	CT, MRI (sagittal/axial T1)	Tumor, T11, T12, L1, L2, L3, L4, L5
5	CT, MRI (sagittal/axial T2), iCT2	Tumor, posterior fixation (screws), T6, T7, T8, T9, T10, T11
6	CT, MRI (sagittal/axial T1, sagittal T2), PET	Tumor, C2, C3, C4, C5, C6, C7, T1, T2, T3, T4, T5, T6, T7, T8, T9, T10, T11, T12, L1, L2, L3, L4, L5
7	MRI (sagittal/axial T2)	Cyst, T11, T12
8	CT, MRI (sagittal T2)	Arachnoid adhesions, spinal cord, T1, T2, T3, T4, T5, T6, T7
9	CT, MRI (sagittal/axial T1, sagittal/axial T2), iCT2, iCT3	Tumor, spinal cord, T5, T6, T7
10	CT, iCT2, iCT3	C7, T2

CT computed tomography, *DWI* diffusion weighted imaging, *iCT* intraoperative computed tomography, *iCT2/iCT3* repeated iCT scans, *iUS* intraoperative ultrasound, *MRI* magnetic resonance imaging, *PET* positron emission tomography

Table 5 Scan length and DLP of scout and registration scan, and total effective dose

No.	Weight (kg)	Scout scan		iCT registration scan					
		DLP (mGy * cm)	Scan length (mm)	Protocol	DLP (mGy * cm)	Scan length (mm)	Level	Total DLP (mGy * cm)	Total ED (mSv)
1	88	9.91	144	C-Spine—70%	87.76	103	C0–C4	97.67	0.53
2	67	31.28	180	Sinus—80%	34.46	120	C0–C4	65.74	0.35
3	80	12.34	192	L-Spine—70%	167.04	167	L1–L4	179.38	3.55
4	78	14.87	242	L-Spine—70%	197.09	213	L1–S1	211.96	4.20
5	85	28.62	231	T-Spine—70%	201.80	197	T5–T11	230.42	4.10
6	70	18.50	131	T-Spine—70%	102.77	102	T5–T8	121.27	2.16
7	70	24.98	195	T-Spine—70%	114.78	120	T11–L2	139.76	2.63
8	95	44.10	384	T-Spine—70%	337.90	321	T2–L2	382.00	6.92
9	95	31.66	261	T-Spine—70%	225.55	197	C7–T8	257.21	4.07
10	95	–*	–*	C-Spine—70%	91.16	109	C6–T3	91.16	0.98

DLP dose length product, *ED* effective dose, *iCT* intraoperative computed tomography

*The scout scan was omitted

for lumbar scans [16, 17]. The DLP refers to a phantom with a diameter of 16 cm in cervical and 32 cm for thoracic and lumbar examinations. In scans covering the cervicothoracic or thoraco-lumbar junction, the conversion factors were weighted according to the amount of vertebra covered.

Augmented reality

For AR support, the heads-up displays of the operating microscopes Pentero/Pentero900 (Zeiss, Oberkochen, Germany) are used. A registration array attached to the microscope allows to track its position (Fig. 1b). For controlling AR calibration, the microscope is centered above the patient reference array, so that the alignment of the AR visualization of the reference array and the optical information can be checked and adjusted if necessary.

Various 3-D objects can be visualized by AR, either in a semitransparent, solid, or outlined fashion. The 3-D objects representing the individual vertebra can be switched on and off for each single vertebra and are generated applying the anatomical mapping software (Brainlab, Munich, Germany). After auto-segmentation, user interaction is needed to fine-tune the segmentation result using a smart brush feature, which is also used to segment the tumor extent. Implants are segmented by thresholding.

Preoperative image data from CT, magnetic resonance imaging (MRI), and positron emission tomography (PET) are fused non-linearly applying the spine

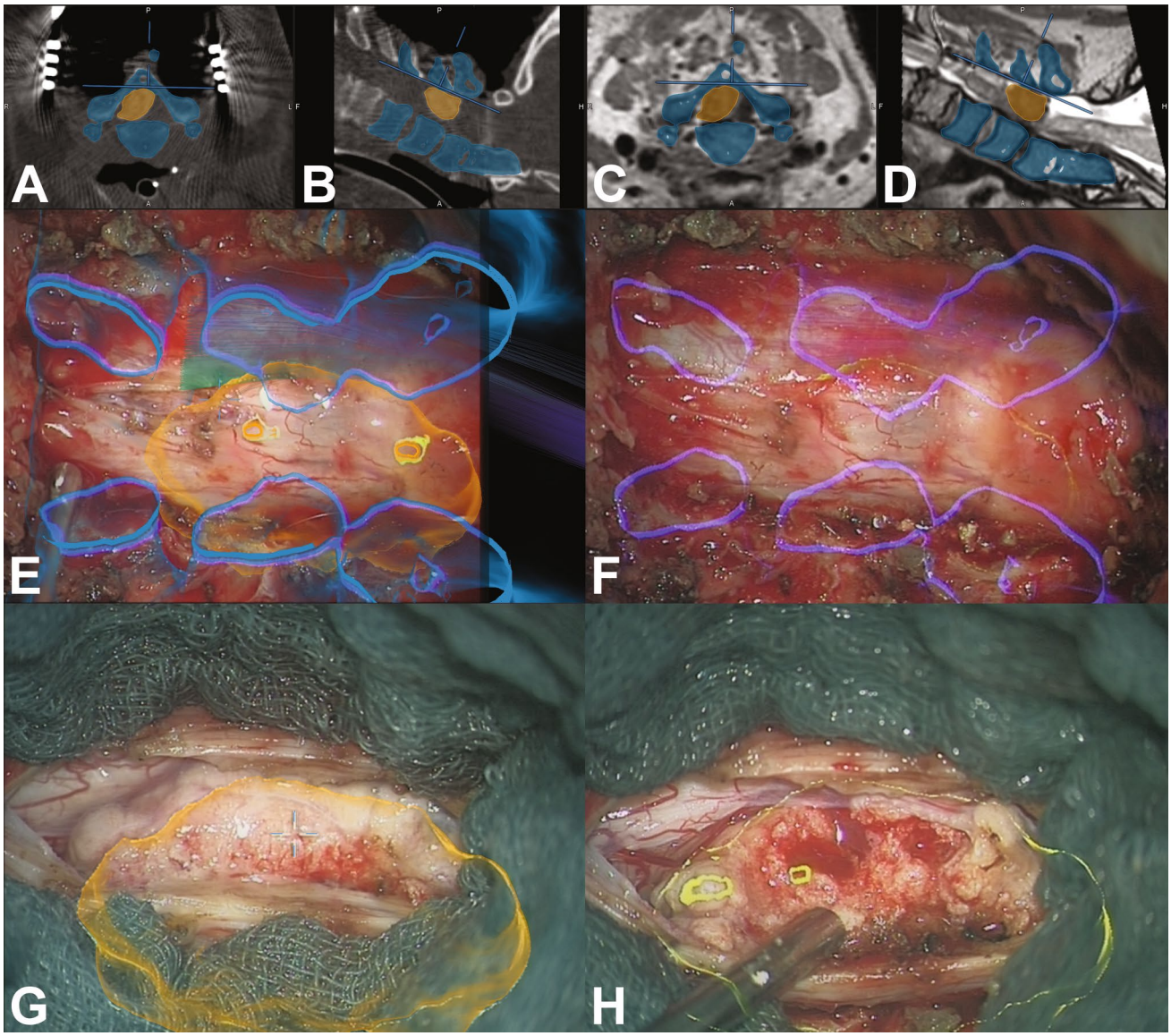

Fig. 3 Calcified intradural meningioma (case no. 1): **a–d** navigation screens, in which the discontinuous blue line represents the viewing axis of the operating microscope, while the perpendicular blue line represents the extent of the optical field of view, the crossing point of both lines is the center of the optical view, visualized in the microscope view as a cross; A/B: inline axial/sagittal view of iCT; **c/d** inline axial/sagittal view of preoperative T2-weighted MRI (C2–C4 are visualized in blue, the tumor extent in yellow); **e–h** AR display prior (**e/f**) (vertebra C2–C4 in blue, tumor extent in yellow) and after dural opening (**g/h**) (only the tumor extent is visualized); **e/g** microscope video displayed on screen with additional overlay of semitransparent objects; **f/h** microscope view as seen by the surgeon in the microscope optics applying the heads-up display

curvature element (Brainlab, Munich, Germany). Preoperative CT and iCT data were used to segment the bony outlines of the vertebra, while co-registered MRI was mostly used to segment the tumor outline due to its much better soft tissue contrast. For landmark checks to verify nonlinear fusion, the segmented vertebra outlines are visualized.

In addition to superimposing the 3-D objects in the operating microscope, the fused datasets are visualized in the spinal navigation application. Furthermore, the microscope application allows to visualize the 3-D objects in a semitransparent or solid mode superimposed to the microscope video; it displays probe's eye views, target views of the 3-D objects, and a 3-D overview depicting how the video frame is positioned in relation to the iCT data (Fig. 1c).

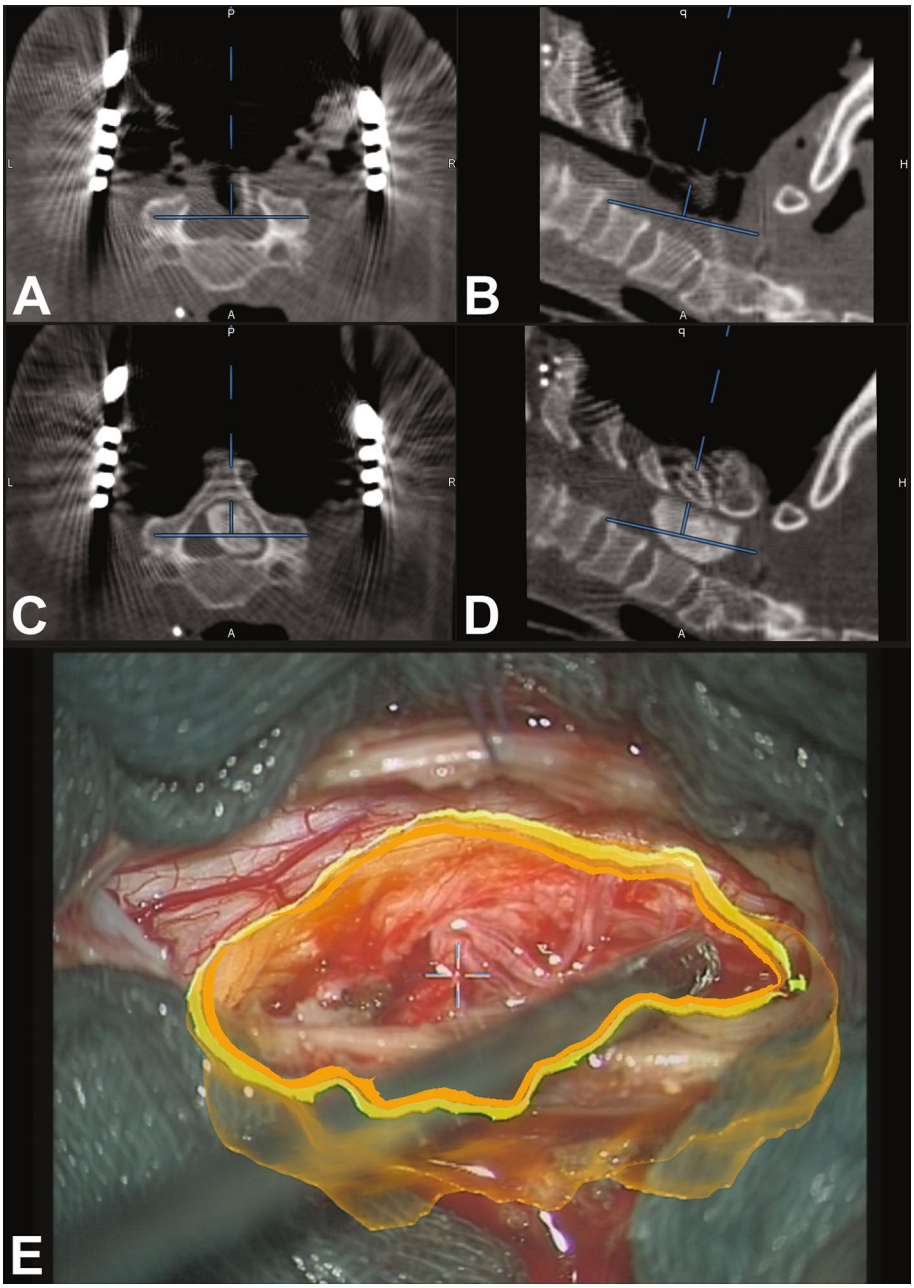

Fig. 4 Same patient as shown in Fig. 3 after repeated iCT for resection control of the calcified meningioma with updated navigation: **a/b** repeated iCT demonstrating the removal of the calcified lesion; **c/d** initial iCT images depicting the tumor; **a/c** inline axial view; **b/d** inline sagittal view; **e** AR display after tumor removal (the tumor extent is visualized in yellow)

Results

Workflow and clinical results

The workflow for establishing AR is straightforward and could be easily integrated into the normal surgical procedure. The entire process of intraoperative registration imaging added only about 5 min to the surgical procedure, and thereafter, AR was instantly available. We did not encounter any technical or surgical problems due to AR implementation. The clinical results are summarized in Table 3.

Registration accuracy

Automatic patient registration without user interaction resulted in high navigation accuracy with a mean registration error of about 1 mm. Different types of anatomical and artificial landmarks allowed to monitor and document accuracy reliably (Fig. 2).

Multimodal image data could be successfully fused nonlinearly with the iCT registration scan. The simultaneous display of the segmented vertebra outlines and fused image datasets while validating the results of automatic fusion proved to be an essential feature. It prevented fusion errors, which otherwise, especially in the mid-thoracic region,

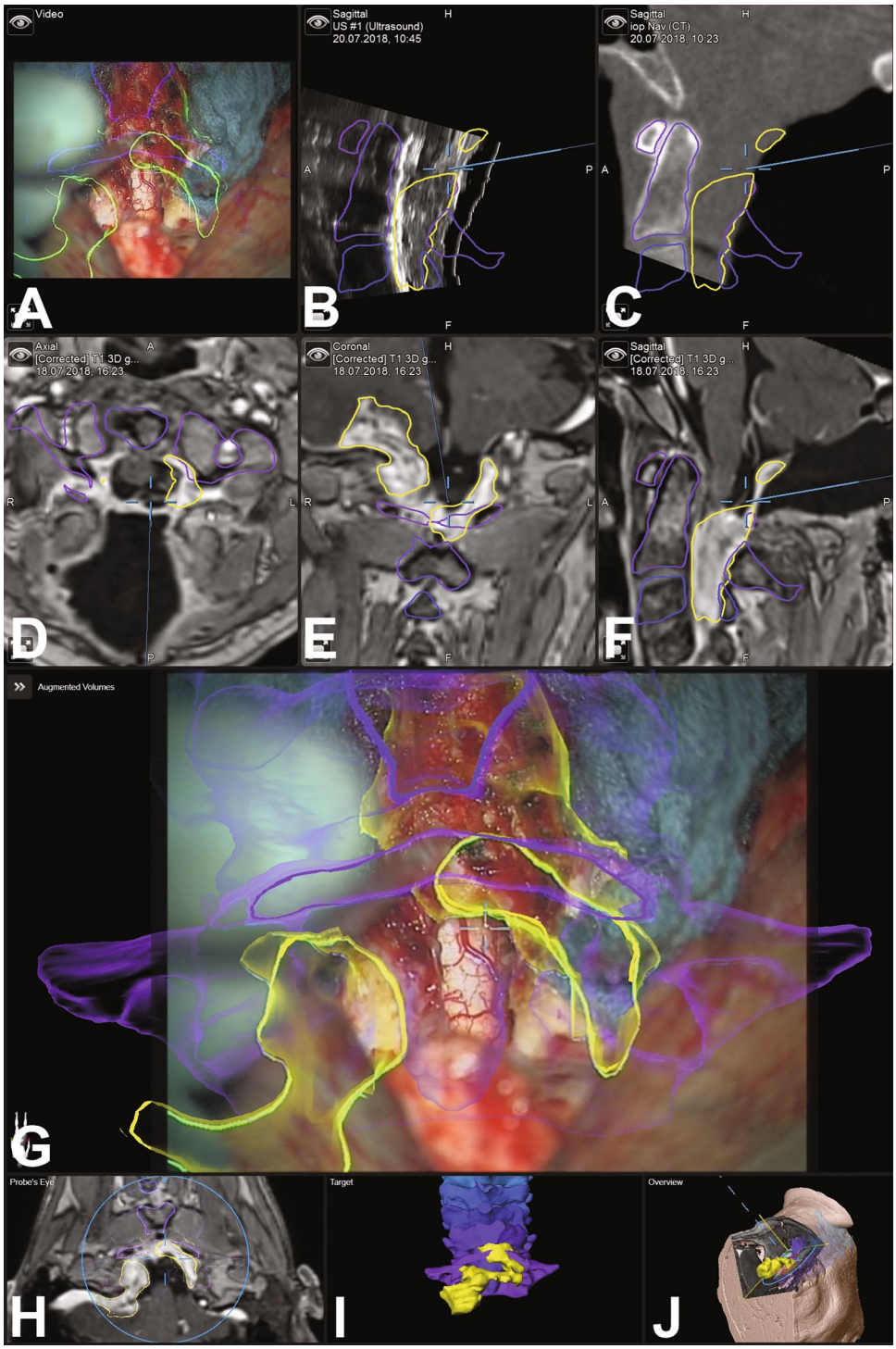

Fig. 5 Intra- and extradural squamous cell lung carcinoma (case no. 2): **a**–**f** navigation screen with **a** microscope video; **b** sagittal reconstruction of co-registered intraoperative 3-D ultrasound; **c** sagittal iCT; **d**–**f** contrast enhanced T1-weighted MRI in axial (**d**), coronal (**e**), and sagittal view (**f**) (the tumor extent is visualized in yellow, C1 and C2 in different shades of violet, C3 in dark blue); **g**–**j** AR display with **g** visualization of the AR volumes as semitransparent objects, **h** a corresponding probe's eye view of the contrast enhanced T1-weighted images, **i** the visualized 3-D objects, **j** a 3-D representation how the video frame is positioned in relation to the MRI data

would have resulted in a nonlinear fusion of non-corresponding vertebra. A pre-adjustment by rigid registration before nonlinear registration was also supportive. In one particular patient (case no. 8), a relatively long iCT scanning range (T2–L2) was necessary, so that level definition for image registration was undoubtedly possible. The final landmark checks ensured high registration accuracy. The image overlay allowing to blend between the different image sets provided additional safety. Table 4 summarizes the fused image sets and the objects visualized in AR.

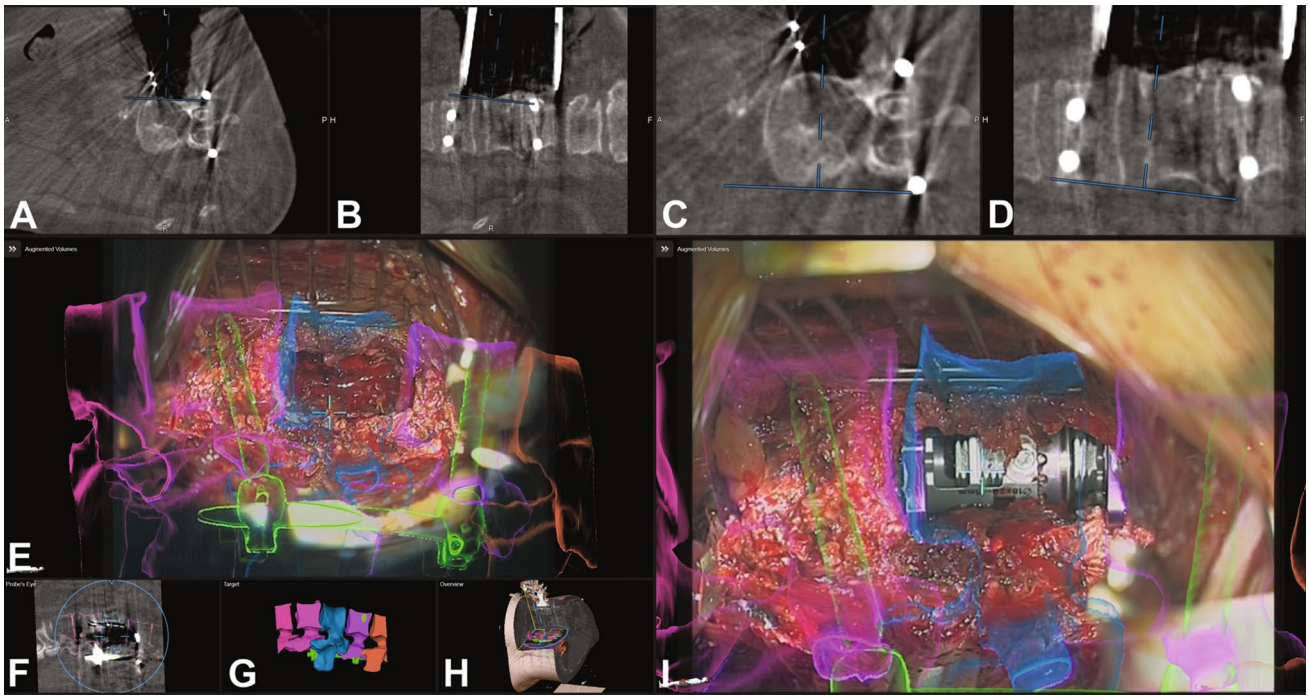

Fig. 6 Breast cancer metastasis in vertebral body L2 (case no. 3): **a**–**d** navigation screen with inline axial (**a/c**) and inline coronal display (**b/d**) at the beginning (**a/b**) and at the end (**c/d**) of corpectomy; **e** AR display after corpectomy; **f** corresponding probe's eye view of iCT; **g** visualized 3-D objects; **h** 3-D representation how the video frame is positioned in relation to the iCT data; **i** AR display with the implanted vertebral body replacement (posterior instrumentation in green, L2 in blue, L3/L4 in shades of pink, L1 in violet, and T12 in orange)

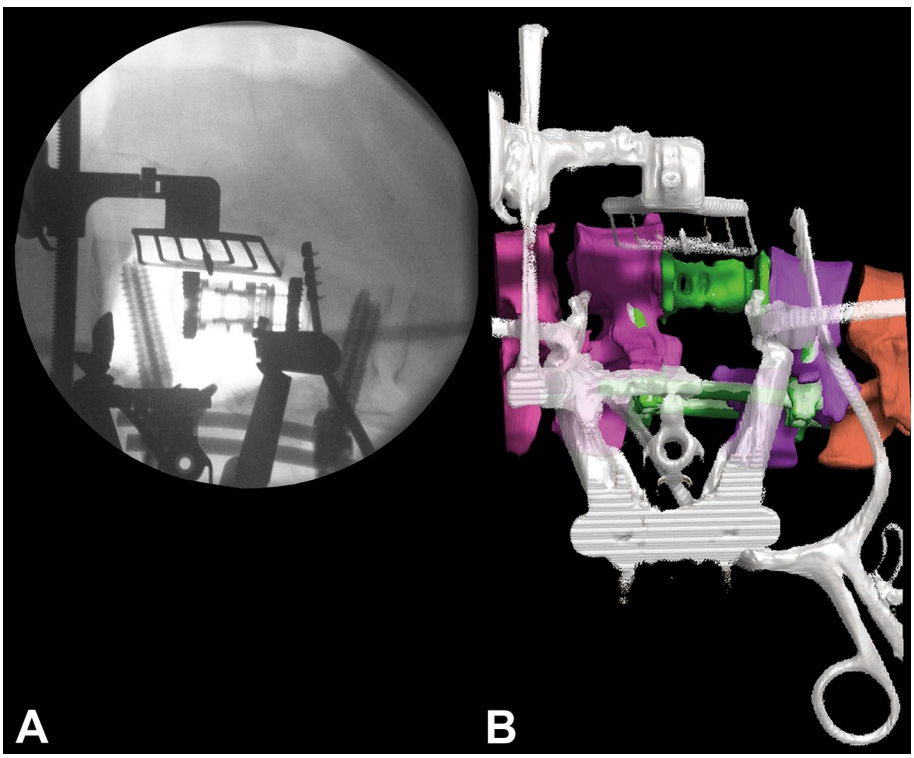

Fig. 7 Same patient as shown in Fig. 6: **a** intraoperative C-arm X-ray after insertion of the expandable vertebral body replacement; **b** corresponding 3-D visualization after repeated iCT, while the implant is also visualized in green

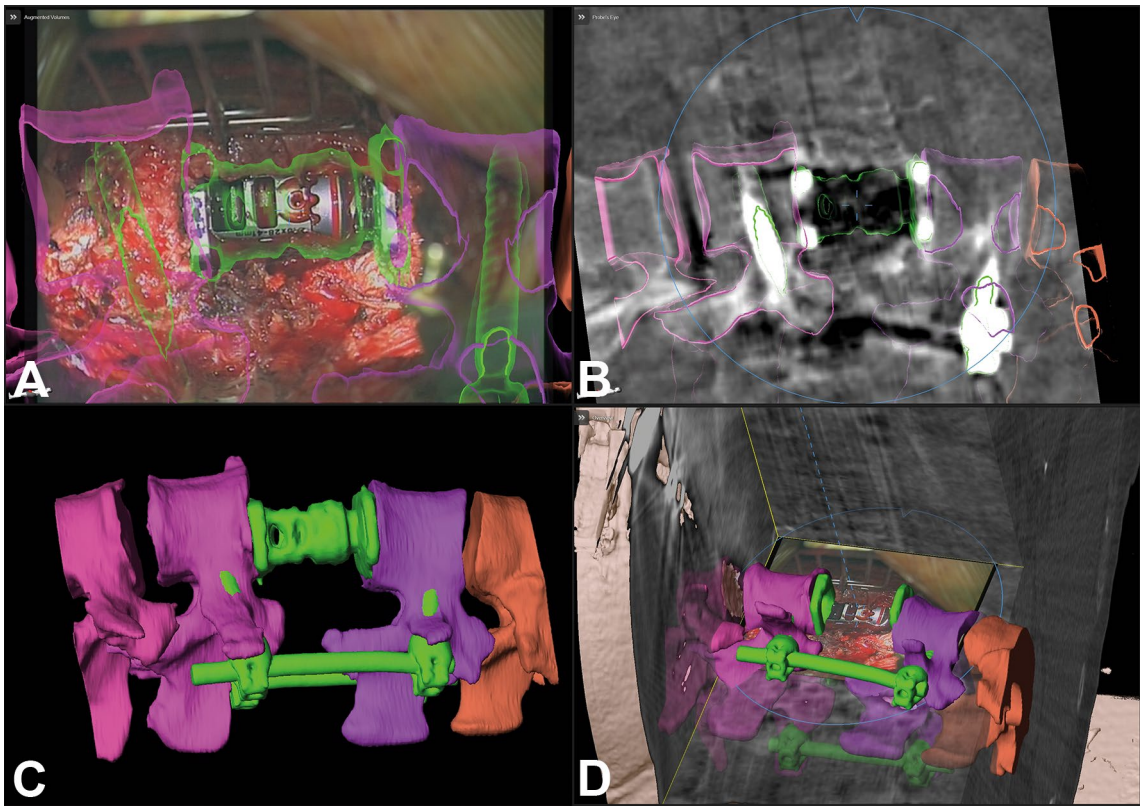

Fig. 8 Same patient as shown in Figs. 6, 7: update of navigation and AR visualization after repeated iCT with the additional visualization of the vertebral body replacement which is segmented in green: **a** AR display demonstrating the close matching of the outline of the vertebral body replacement and its augmented representation; **b** probe's eye view; **c** visualized 3-D objects; **d** 3-D representation how the video frame is positioned in relation to the iCT data

Effective dose

The scan range of iCT was defined by the surgical exposure of the spine. This minimized scan length and therefore radiation exposure. Low-dose iCT protocols resulted in a total effective radiation dose of 0.35–0.98 mSv for cervical, 2.16–6.92 mSv for thoracic, and 3.55–4.20 mSv for lumbar procedures (Table 5), which is a reduction in the effective radiation dose compared to a standard spinal helical scan by about 70%.

Augmented reality

The segmented structures (Table 4) were intuitively visualized in the surgical field by AR (Figs. 3, 4, 5, 6, 7, 8, 9, 10, 11). There was a very good calibration correspondence of the AR overlay displayed directly in the microscope view with the AR superimposed on the microscope video (Figs. 3e/f, g/h, 5a/g). On request of the surgeon, the heads-up display in the operating microscope was turned on or off, preventing that too much information resulted in a distraction from the actual surgical field. Depending on the surgical situation, selected objects were displayed optionally, so, e.g., after laminectomy the outline of the vertebra was sometimes switched off to solely visualize the tumor (Fig. 10g/h). Implants (screws or vertebral body replacements) served as ideal control to check the accuracy of AR, showing a very close matching between superimposed visualization and real structure (Figs. 8, 9). In parallel, the microscope video display superimposed with AR along with various representations of the image data (Fig. 11a/d) helped the surgeon to maintain orientation even when microscope AR was switched off for an undisturbed view of the surgical field. This display also helped the assisting staff to precisely follow the procedure and is a valuable tool for education. Moreover, the overview display depicting the 3-D representation how the video frame is positioned relative to the iCT data (Figs. 5j, 8d, 10e/f) helped to understand microscope alignment.

Discussion

AR for spine surgery was successfully implemented in a clinical setting. Thus, all benefits that are common place in cranial neurosurgery when applying heads-up displays

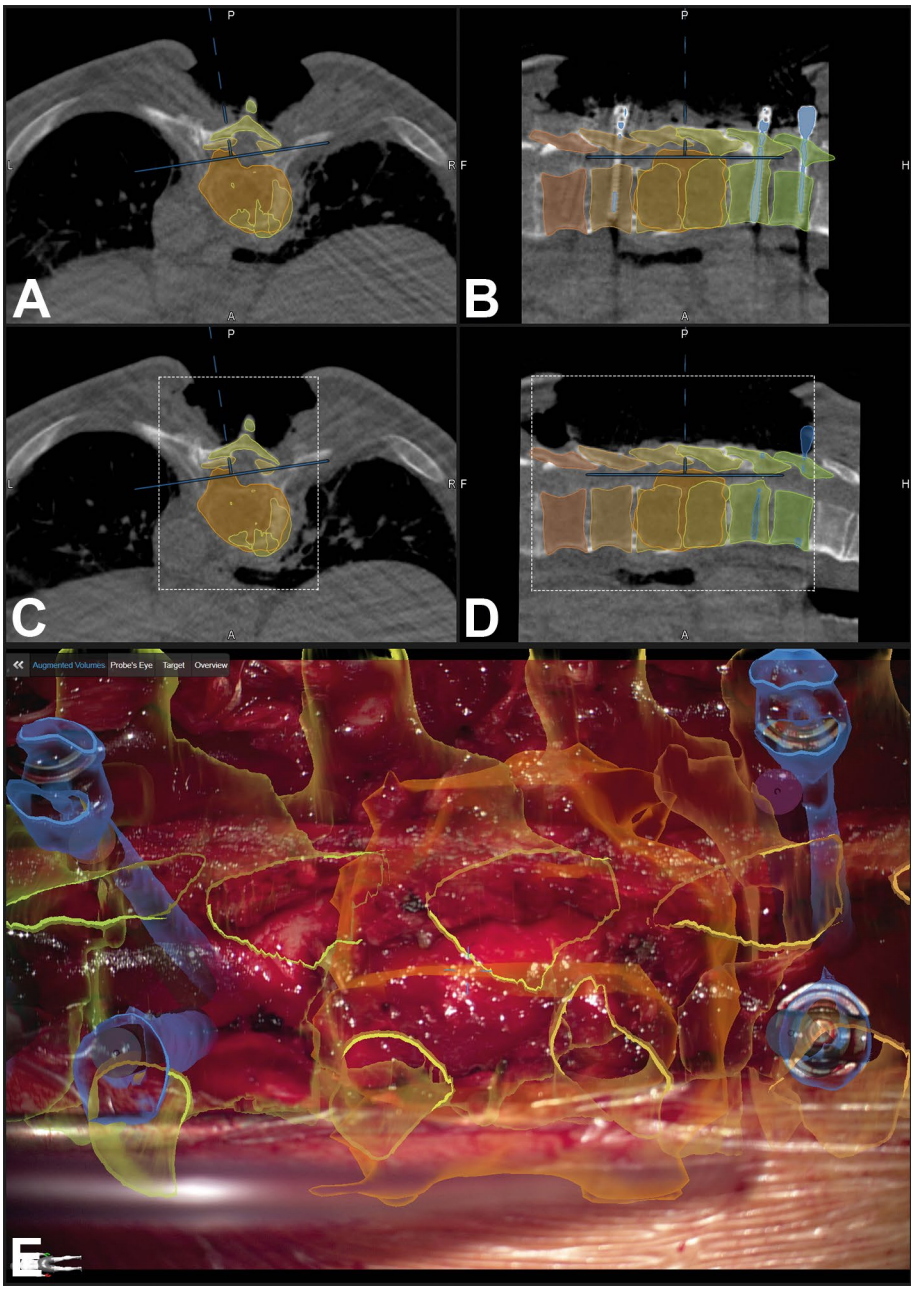

Fig. 9 Small cell lung carcinoma metastasis in T8 and T9 (case no. 5): **a/b** repeated iCT after navigated placement of pedicle screws; **c/d** initial iCT for navigation registration; **e** AR display demonstrating the close matching of the screw heads and their AR visualization (blue objects)

of operating microscopes for AR are now also available for spinal applications. This technology offers new avenues of supporting the spine surgeon in various surgical situations.

AR enhanced the understanding of 3-D anatomy and facilitated surgery greatly. Further, AR will distinctly increase the comfort for the surgeon especially in situations, when anatomical landmarks are lacking, such as in reoperations. Also, there is a huge potential as educational tool. We did not encounter a learning curve in this small series, which is probably due to the fact that our team is well experienced with microscope-based AR support in cranial neurosurgery. Using the heads-up displays of the operating microscopes for AR support ensures that the surgical workflow and hand–eye coordination are not disturbed. On the other hand, it has to be ensured that the AR display does not distract the surgeon from the actual surgical field. AR support should be able to selectively display the necessary information adjusted to a surgical step, and AR should be easily switched off enabling an undisturbed view of the surgical field. The combination with virtual reality-based simulators might be beneficial [18].

Another advantage of AR is a facilitated identification of the tumor extent by visualizing the tumor outline in the surgical field. Even in cases when the registration accuracy

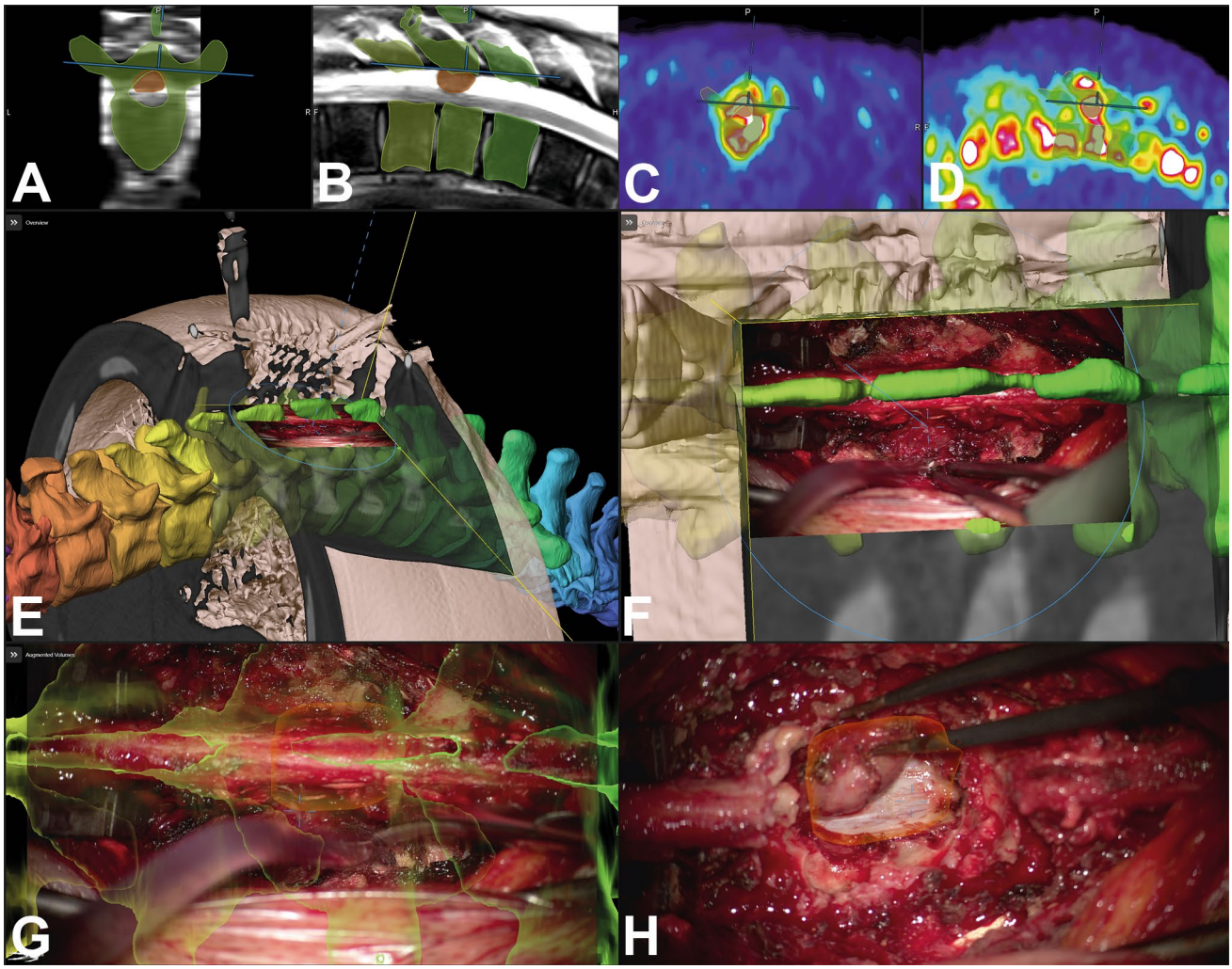

Fig. 10 Epidural neuroendocrine carcinoma metastasis T6 (case no. 6): **a**–**d** navigation screen with inline axial (**a/c**) and inline sagittal display (**b/d**) of T2-weighted MRI (**a/b**) and PET (**c/d**) (vertebra T5–T7 and tumor extent are segmented); **e/f** different viewing angles of the 3-D representation how the video frame is positioned in relation to the iCT data and the visualized objects; **g/h** AR display prior laminectomy (**g**) and after (**h**); in (**h**) the tumor is just lifted away from the dura

is compromised due to some positional shifting, e.g., by an accidental movement of the patient reference array, the size of an object is still displayed correctly, so that the extent of a tumor can be well estimated by the surgeon. Anatomical landmarks or implants such as screws or vertebral body replacements provide an ideal opportunity to check registration accuracy, as well as a possibility to correct registration errors by adjusting the projected outlines if necessary.

Besides tumor surgery, also surgery of vascular spinal lesions might also greatly benefit from AR, especially when these techniques are further enhanced by intraoperative Doppler ultrasound and fluorescence angiography techniques, such as in cranial vascular neurosurgery [7–9]. Also for degenerative spine and spine trauma surgery AR might offer support as demonstrated in phantom studies for pedicle screw placements [12, 13] and visualization of cutting lines for osteotomies [14]. Minimal invasive spine surgery often has the challenge of a long learning curve due to an obscured anatomical orientation during surgery, e.g., when applying endoscopes. AR has a huge potential to impact and enhance minimally invasive spine surgery.

Intraoperative imaging is key for a highly reliable patient registration. The concept of user-independent registration, based on intraoperative imaging, reduces registration errors [15]. iCT is the most suitable imaging modality for spine registration since it allows a clear delineation of bony landmarks and structures. The registration error in our series of patients, measured by different approaches, like identifying anatomical or artificial landmarks was in the range of 1 mm, which corresponds well to a target registration error in cranial procedures of 0.93 ± 0.41 mm when applying iCT for automatic registration [15]. In case the registration

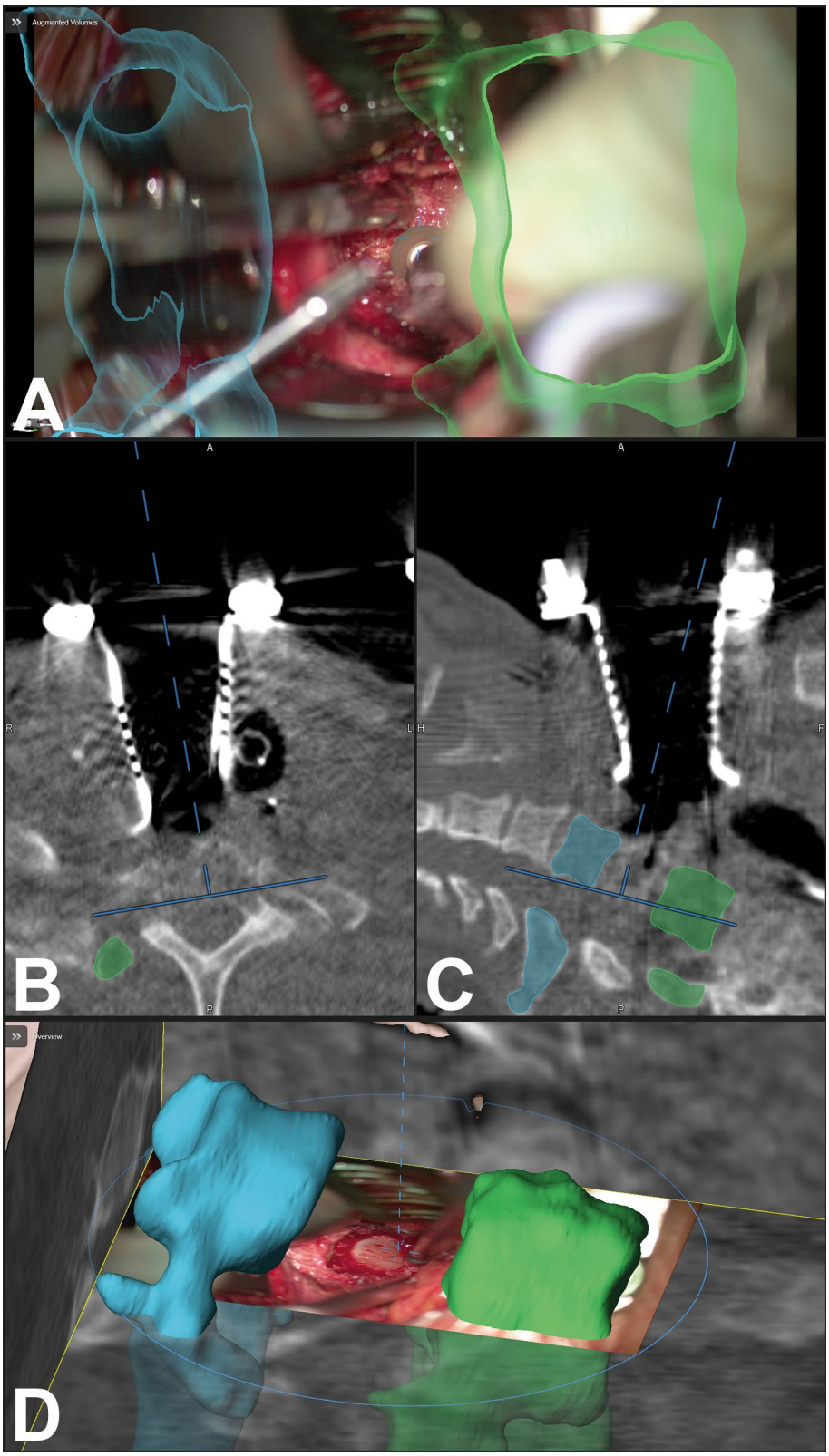

Fig. 11 Small cell lung carcinoma metastasis in T1 (case no. 10): anterior approach for corpectomy of T1, in the AR display (**a**) the adjacent vertebra C7 (blue) and T2 (green) are visualized as semitransparent objects; **b/c** navigation screen with inline axial and inline sagittal display of iCT; **d** AR display after corpectomy with the ventral dura visible (C7 and T2 visualized as solid objects)

scan is performed after bone removal, e.g., after laminectomy, the highest precision can be expected, since no further movement occurs. The sagittal alignment is not altered after registration scanning, when the patient is placed carefully on the operating table with adequate support. Repeated landmark checks ensure persisting navigational precision, and

the system provides additional safety by warning the surgeon in case movements of the registration array are detected, thus allowing to check landmarks or performing a repeated registration scan. The overall application error of AR not only depends on the patient registration error but also on the accuracy of image fusion which is very high in lesions that are clearly visible in iCT but might add up to 1–2 mm of inaccuracy in others. iCT for AR navigation registration was smoothly integrated into the surgical workflow and added only about 5 min to the whole procedure.

Since CT imaging poses the risk of cancer induction, we applied low-dose protocols which led to a reduction in the effective dose by about 70% compared to the standard spinal protocols. Furthermore, restricting the scan region to the surgical exposure further minimizes radiation exposure by reducing iCT scan length. However, in cases with few prominent anatomical or artificial landmarks, especially in the mid-thoracic region, the iCT scan must cover a longer range of vertebra, so that the preoperative image data can be fused reliably.

With the low-dose iCT protocols, we achieved effective doses of 0.35–0.98 mSv for cervical, 2.16–6.92 mSv for thoracic, and 3.55–4.20 mSv for lumbar surgeries. A recent literature review reported effective doses for spine CT of 10.3 mSv (range 4.0–16.7 mSv) [19]. It is important to find the clinical threshold where decreasing image quality for reduction in radiation exposure still does not impede the usability of the images [20, 21]. With regard to iCT for patient registration, further dose reduction might be possible until a principle limit is reached when the increased image noise prevents a reliable fusion with other image datasets.

A radiation-free alternative for registration could be the point matching procedure, where the pointer is used to build a 3-D surface model of the vertebra lamina for registration. The major drawback is that this can only be used reliably for single vertebra applications due to the flexibility in sagittal and lateral alignment. Another alternative for radiation-free registration might be intraoperative ultrasound [13]; however, until now, clinical feasibility and acceptable accuracy could not be demonstrated. In a study performing a multi-vertebrae CT-ultrasound registration, an initial registration error of up to 25 mm could be reduced to a mean error of 1.37 mm. However, deviations of up to 5 mm in individual cases [22] show still insufficient reliability.

Challenges in navigation like those known from cranial neurosurgery also apply for spine navigation. Shifting of the spinal cord occurs when it is decompressed, and the tumor mass is removed. In these cases, a potential solution might be integration of intraoperative 3-D ultrasound allowing an update of navigation, as repeated iCT. Since low-dose protocols are implemented, repeated scanning can be performed with reasonable radiation exposure, particularly if the scan length is restricted to the area of interest.

We are aware of limitations in our study that are due to the preliminary nature of this report. However, we are demonstrating proof of concept for improvement in surgery using AR. The actual individual patient benefit due to AR, however, is difficult to quantify objectively. Despite the small number of patients, we could demonstrate a consistent high reliability of AR support due to automatic iCT-based registration.

Currently, AR rapidly gains interest in different surgical disciplines. However, until now the clinical application in spine surgery is still in its infancy. Without doubt, this technology will find its way into routine clinical applications, while optimal solutions need to be further developed. There are different approaches to implement AR with devices integrated in glasses [23] or phone [24] or tablet-like handheld devices or mounted above the surgical field [25], when no operating microscope is available, or the operating microscope is not needed. The upcoming concept of exoscopes, developed and investigated by several manufacturers, will also promote AR. It is therefore likely that not only the AR devices have to be adapted to the surgical procedure, but also the surgical procedure itself will be changed by AR resulting in more minimally invasive procedures, even including the integration of robotic systems supported by AR.

Conclusions

A microscope-based AR environment was successfully implemented for spinal surgery. Applying iCT for registration imaging allowed user-independent registration and ensures high navigational accuracy. AR greatly supports the surgeon in understanding the 3-D anatomy, thereby facilitating surgery. Using the implemented technique and workflow offers a wide variety of potential applications for AR support in spinal surgery.

Acknowledgements We would like to thank J.-W. Bartsch for thoroughly proofreading the manuscript.

Compliance with ethical standards

Conflict of interest B Carl, M. Bopp, B. Saß and B. Voellger declare that they have no conflict of interest. Ch. Nimsky received speaker fees from Brainlab.

References

1. Kelly PJ, Alker GJ Jr, Goerss S (1982) Computer-assisted stereotactic microsurgery for the treatment of intracranial neoplasms. Neurosurgery 10(3):324–331
2. Roberts DW, Strohbehn JW, Hatch JF, Murray W, Kettenberger H (1986) A frameless stereotaxic integration of computerized

tomographic imaging and the operating microscope. J Neurosurg 65(4):545–549. https://doi.org/10.3171/jns.1986.65.4.0545
3. Kiya N, Dureza C, Fukushima T, Maroon JC (1997) Computer navigational microscope for minimally invasive neurosurgery. Minim Invasive Neurosurg 40(3):110–115. https://doi.org/10.1055/s-2008-1053429
4. Nimsky C, Ganslandt O, Kober H, Moller M, Ulmer S, Tomandl B, Fahlbusch R (1999) Integration of functional magnetic resonance imaging supported by magnetoencephalography in functional neuronavigation. Neurosurgery 44(6):1249–1255. https://doi.org/10.1097/00006123-199906000-00044
5. Barnett GH, Steiner CP, Weisenberger J (1995) Adaptation of personal projection television to a head-mounted display for intra-operative viewing of neuroimaging. J Image Guided Surg 1(2):109–112. https://doi.org/10.1002/(sici)1522-712x(1995)1:2%3c109:Aid-igs6%3e3.3.Co;2-m
6. Masutani Y, Dohi T, Yamane F, Iseki H, Takakura K (1998) Augmented reality visualization system for intravascular neurosurgery. Comput Aided Surg 3(5):239–247. https://doi.org/10.3109/10929089809149845
7. Cabrilo I, Bijlenga P, Schaller K (2014) Augmented reality in the surgery of cerebral aneurysms: a technical report. Neurosurgery 10(Suppl 2):252–260. https://doi.org/10.1227/neu.0000000000000328 **(discussion 260-251)**
8. Cabrilo I, Sarrafzadeh A, Bijlenga P, Landis BN, Schaller K (2014) Augmented reality-assisted skull base surgery. Neurochirurgie 60(6):304–306. https://doi.org/10.1016/j.neuchi.2014.07.001
9. Carl B, Bopp M, Chehab S, Bien S, Nimsky C (2018) Preoperative 3-dimensional angiography data and intraoperative real-time vascular data integrated in microscope-based navigation by automatic patient registration applying intraoperative computed tomography. World Neurosurg 113:e414–e425. https://doi.org/10.1016/j.wneu.2018.02.045
10. Abe Y, Sato S, Kato K, Hyakumachi T, Yanagibashi Y, Ito M, Abumi K (2013) A novel 3D guidance system using augmented reality for percutaneous vertebroplasty: technical note. J Neurosurg Spine 19(4):492–501. https://doi.org/10.3171/2013.7.SPINE12917
11. Agten CA, Dennler C, Rosskopf AB, Jaberg L, Pfirrmann CWA, Farshad M (2018) Augmented reality-guided lumbar facet joint injections. Invest Radiol 53(8):495–498. https://doi.org/10.1097/RLI.0000000000000478
12. Elmi-Terander A, Skulason H, Soderman M, Racadio J, Homan R, Babic D, van der Vaart N, Nachabe R (2016) Surgical navigation technology based on augmented reality and integrated 3D intraoperative imaging: a spine cadaveric feasibility and accuracy study. Spine (Phila Pa 1976) 41(21):E1303–E1311. https://doi.org/10.1097/brs.0000000000001830
13. Ma L, Zhao Z, Chen F, Zhang B, Fu L, Liao H (2017) Augmented reality surgical navigation with ultrasound-assisted registration for pedicle screw placement: a pilot study. Int J Comput Assist Radiol Surg 12(12):2205–2215. https://doi.org/10.1007/s11548-017-1652-z
14. Kosterhon M, Gutenberg A, Kantelhardt SR, Archavlis E, Giese A (2017) Navigation and image injection for control of bone removal and osteotomy planes in spine surgery. Oper Neurosurg (Hagerstown) 13(2):297–304. https://doi.org/10.1093/ons/opw017
15. Carl B, Bopp M, Sass B, Nimsky C (2018) Intraoperative computed tomography as reliable navigation registration device in 200 cranial procedures. Acta Neurochir (Wien) 160(9):1681–1689. https://doi.org/10.1007/s00701-018-3641-6
16. Huda W, Ogden KM, Khorasani MR (2008) Converting dose-length product to effective dose at CT. Radiology 248(3):995–1003. https://doi.org/10.1148/radiol.2483071964
17. Elbakri IA, Kirkpatrick ID (2013) Dose-length product to effective dose conversion factors for common computed tomography examinations based on Canadian clinical experience. Can Assoc Radiol J 64(1):15–17. https://doi.org/10.1016/j.carj.2011.12.013
18. Pfandler M, Lazarovici M, Stefan P, Wucherer P, Weigl M (2017) Virtual reality-based simulators for spine surgery: a systematic review. Spine J 17(9):1352–1363. https://doi.org/10.1016/j.spine.2017.05.016
19. Vilar-Palop J, Vilar J, Hernandez-Aguado I, Gonzalez-Alvarez I, Lumbreras B (2016) Updated effective doses in radiology. J Radiol Prot 36(4):975–990. https://doi.org/10.1088/0952-4746/36/4/975
20. Greffier J, Pereira FR, Viala P, Macri F, Beregi JP, Larbi A (2017) Interventional spine procedures under CT guidance: how to reduce patient radiation dose without compromising the successful outcome of the procedure? Phys Med 35:88–96. https://doi.org/10.1016/j.ejmp.2017.02.016
21. Sarwahi V, Payares M, Wendolowski S, Maguire K, Thornhill B, Lo YT, Amaral TD (2017) Low-dose radiation 3D Intraoperative imaging how low can we go? An O-arm, CT scan, cadaveric study. Spine 42(22):E1311–E1317. https://doi.org/10.1097/Brs.0000000000002154
22. Nagpal S, Abolmaesumi P, Rasoulian A, Hacihaliloglu I, Ungi T, Osborn J, Lessoway VA, Rudan J, Jaeger M, Rohling RN, Borschneck DP, Mousavi P (2015) A multi-vertebrae CT to US registration of the lumbar spine in clinical data. Int J Comput Assist Radiol Surg 10(9):1371–1381. https://doi.org/10.1007/s11548-015-1247-5
23. Yoon JW, Chen RE, Kim EJ, Akinduro OO, Kerezoudis P, Han PK, Si P, Freeman WD, Diaz RJ, Komotar RJ, Pirris SM, Brown BL, Bydon M, Wang MY, Wharen RE Jr, Quinones-Hinojosa A (2018) Augmented reality for the surgeon: systematic review. Int J Med Robot 14(4):e1914. https://doi.org/10.1002/rcs.1914
24. Hou Y, Ma L, Zhu R, Chen X, Zhang J (2016) A low-cost iPhone-assisted augmented reality solution for the localization of intracranial lesions. PLoS ONE 11(7):e0159185. https://doi.org/10.1371/journal.pone.0159185
25. Watanabe E, Satoh M, Konno T, Hirai M, Yamaguchi T (2016) The trans-visible navigator: a see-through neuronavigation system using augmented reality. World Neurosurg 87:399–405. https://doi.org/10.1016/j.wneu.2015.11.084

Affiliations

Barbara Carl[1] · Miriam Bopp[1,2] · Benjamin Saß[1] · Benjamin Voellger[1] · Christopher Nimsky[1,2]

[1] Department of Neurosurgery, University Marburg, Baldingerstrasse, 35033 Marburg, Germany

[2] Marburg Center for Mind, Brain and Behavior (MCMBB), Marburg, Germany